Human Proximity Effects on Circular Polarized Handset Antennas in Personal Satellite Communications

Joseph S. Colburn, *Student Member, IEEE*, and Yahya Rahmat-Samii, *Fellow, IEEE*

***Abstract*— Satellite-based systems are the next step in mobile communications. Recently, several low and medium earth orbit mobile communication satellite systems have been proposed and are currently being deployed. For all these systems, high-performance circularly polarized antennas for the mobile terminals are of importance. Although considerable material is available on circularly polarized antennas, there is an absence of information on how the human's close proximity to the antenna affects the circular polarization purity of the radiated field. This paper presents an analysis of representative circularly polarized helical handset antennas. Although other physically less obtrusive circular polarized antennas are available for the handset, the helix is used because of its wide bandwidth properties and capability to provide both circular and linear polarization. Thus, this element could be used for handsets that are planned to work with both the terrestrial-based communications systems of today and the satellite-based communication systems of tomorrow. The intent is to characterize the effects the close proximity of a human head model has on the computed performance of the circular polarized antenna. The method of moments (MoM) and finite-difference time-domain (FDTD) numerical techniques are used to study various helix structures on top of a small box representing a handset. In order to be able to effectively apply FDTD, a novel square helix structure is introduced. Results computed with these two techniques are compared to illustrate the accuracy of each implementation. The results indicate significant polarization purity degradation caused by the presence of a human head. For the particular geometry simulated, the presence of a head model degraded the average axial ratio within a verticle 50° cone from 2.9 to 9.1 dB. This significant increase in axial ratio can have profound effects on link budgets.**

***Index Terms*— Circular polarization, FDTD, helical antennas, human interactions, MoM, satellite communication.**

I. Introduction

PRESENTLY, several multibillion dollar global mobile satellite communication systems are under development, some of which are scheduled to be operational within a year's time. The intent of these satellite-based systems is to provide seamless worldwide communications coverage. Although the development cost of these systems are very high, the market potential for the services provided is tremendous. The technology needed to implement these systems is of critical importance for their success.

Manuscript received April 4, 1997; revised March 5, 1998. This work was supported in part by Rockwell/Micro contract at UCLA.

The authors are with the Department of Electrical Engineering, University of California, Los Angeles, CA 90095 USA.

Publisher Item Identifier S 0018-926X(98)04871-6.

The majority of the systems suggested for the global mobile satellite communications markets fall under the "Big LEO" or "Big MEO" title [1], [2]. "Big" in this classification refers to the property that the systems would have enough power and bandwidth to provide real time high-fidelity voice and data transmission capabilities. The "LEO" or "MEO" designation refers to the satellite orbit—"LEO" meaning low earth orbit and "MEO" meaning medium earth orbit. All these systems use the L- and/or S-band for up and down links to the mobile terminal, employing circular polarization. The low and medium earth orbits necessitate wide viewing angles for the mobile terminal to guarantee visibility of at least one satellite at all times due to the satellite's motion in the user's reference frame. High-performance radiation and circuit characteristics are required of the handset antenna in order to maintain acceptable communication link margins. Two challenges for the mobile satellite communications system handset antenna include broad radiation patterns with good axial ratio performance and widely separated transmit and receive frequency bands. Additional complexity is introduced by the fact that the handset will be in close proximity to a human operator, which can result in significant electromagnetic interactions. This paper addresses the issue of coupling between the handset operator and the circular polarized handset antenna by presenting numerical results for a representative antenna configuration.

In this work, results from the study of one candidate antenna for a personal satellite transceiver handset—a thin-wire helix antenna—are detailed. Many physically less-obtrusive circular polarized antennas have been studied for the handset application [3], [4], but the helix antenna is considered a good candidate element because it can provide wide-band impedance performance with acceptable circular polarization when operated in axial mode. An additional benefit of the helix is that at lower frequencies it can provide linear polarization when operated in normal mode. This property could be exploited for handsets that intend to take full advantage of both satellite and terrestrial systems coverage.

The helix antenna is analyzed through a series of numerical simulations. A traditional circular helix mounted on a small perfect electrical conducting box is first analyzed by method of moments (MoM) and its circular polarization-radiation characteristics shown. Next, the development of a novel square helix is addressed. Besides the possible benefit of integrating the square version of the helix with a handset, this type of radiator can be simulated with a Cartesian grid finite-difference

time-domain (FDTD) code. The square helix with the best circular radiation performance is analyzed with both Cartesian grid FDTD and MoM and those results are directly overlayed to provide a unique comparison of these two popular full-wave analysis techniques.

The effects of a human's presence on the radiation characteristics of this circularly polarized antenna and the effects of radiated fields from the antenna on human tissue are presented last. This involves positioning a computational head model near the handset in the FDTD computational domain, then calculating the resulting radiation and circuit performance. The major emphasis of this paper will be to explore depolarization of the far-field radiation caused by the head model. The inhomogeneous head model used in these FDTD computations consists of approximately 12 000 Yee cells with 3.33-mm resolution. Although more detailed head models could have been used, for the far-field polarization emphasis of this study the head model has sufficient resolution. Computed near-field distributions around the antenna and head model and specific absorption rate (SAR) values in the head model are shown.

II. Numerical Techniques

In this work, both the MoM and FDTD numerical techniques are used to analyze various helix structures. These full-wave techniques are considerably different in origin, thus, the use of the two provide diversity in simulation capabilities and independent verification of results.

A. MoM

The MoM technique [5] is a current-based integral equation approach for solving Maxwell's equations. A substantial amount of research has been conducted on MoM and the technique has matured into a very flexible full-wave simulation tool [6]. The Rao *et al*. basis functions [7] and thin-wire approximations [8], [9] allow considerable freedom in modeling planar conductors and wire structures. Sophisticated combined electric-field and magnetic-field integral equation formulations have been developed [10] that can handle arbitrary three-dimensional bodies. The volume integral equation approach of modeling complex inhomogeneous dielectrics [11] has been coupled to thin-wire modeling approaches to simulate wire antennas near dielectric material [12], [13]. The accuracy and modeling flexibility of this method are its significant strengths.

The disadvantage of this technique is the numerical cost, which grows at least as the square of the electrical size of the problem. This numerical cost gets prohibitively expensive when attempting to accurately model a computation head in close proximity to a radiator [12], [13] at frequencies of interest for the mobile satellite communication links.

B. FDTD

The FDTD technique is a field-based approach for solving Maxwell's equations in differential form with center difference approximation in both time and space [14]. Similar to the MoM technique, considerable research has advanced this method to the point where it has wide application in full-wave electromagnetics modeling [15]. This technique readily handles planar conductors, thin wires, and inhomogeneous dielectrics [16]. It has been used extensively in studying the effects close proximity of a human head has on the performance of transceiver handsets for terrestrial mobile systems [17]–[21].

The most common and simplest form of FDTD is based on a Cartesian coordinate system discretization, which limits the geometries that can be studied. FDTD based on nonuniform discretization has been developed, but this flexibility comes at the cost of increased complexity, increased numerical cost, and decreased accuracy [16]. This is especially true for geometries that deviate significantly from uniform Cartesian grids such as the traditional circular helix.

III. Helices on Handset

Helix antennas are presently considered one the most practical antenna element for the personal satellite communications handset. This well-studied radiator can provide good circular polarization and low return loss over a considerable bandwidth. Past research on the helix antenna, however, did not address the effects of a small handset or close proximity of a human operator has on the electrical performance of the helix. These issues are explored with the MoM and FDTD numerical techniques mentioned in the two following sections. Much of the results to be presented were calculated at 1.8 GHz. This frequency is emphasized because it falls close to the transmit and receive bands (L and/or S band) of the proposed personal satellite systems, thus providing results characteristic of both bands.

First, a circular helix mounted on a small handset is studied with the MoM technique. Following that, results for a square version of the helix are presented and it is shown that this radiator has circuit and radiation characteristics similar to the circular helix. The square helix was simulated with both MoM and FDTD. The results of the two techniques are compared in order to gain confidence in the computed results. Because of the different origins of the MoM and FDTD techniques, comparison of results generated with the two methods provide an independent verification of the simulations. The final set of results presented are simulations of the square helix antenna in close proximity to a computation head model. These results were generated with the FDTD technique.

A. Circular Helix on Handset

Fig. 1 is a schematic of a helix antenna mounted on a small transceiver box. The radiator is a standard four-turn helix [22] (diameter $= 0.306\lambda$, $0.001\,395\lambda$ wire radius, pitch angle $= 14°$) mounted on a $0.48\lambda \times 0.48\lambda \times 0.8\lambda$ conducting box. At 1.8 GHz, the box dimensions are 8 cm $\times$ 8 cm $\times$ 13.33 cm and the helix diameter $= 5.1$ cm. Although this geometry is large for a handset, this work did not try to determine the best handset design, but intended to be a representative case study to explore polarization-degradation issues of the mobile satellite communication handset antenna.

The circular helix structure described in Fig. 1 was analyzed by the MoM. Fig. 2(a) and (b) plots the MoM-computed far-field pattern and axial ratio, respectively. The far-field pattern is plotted in terms of right-hand circularly polarized (RHCP)

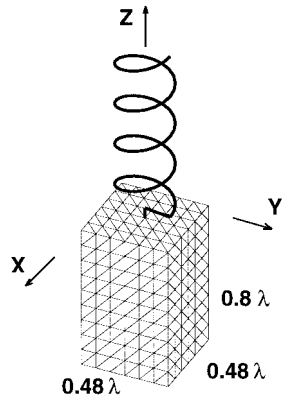

Fig. 1. Schematic of a standard helix (diameter $= 0.306\lambda$, pitch angle $= 14°$, wire radius $= 0.001\,395\lambda$) mounted on a $0.48\lambda \times 0.48\lambda \times 0.8\lambda$ conducting box ($\lambda = 16.7$ cm at 1.8 GHz).

and left-hand circularly polarized (LHCP) components. From this plotted far-field pattern data, one can see this handset radiator has fairly good circular polarization performance. In fact, within the 50° vertical cone the average axial ratio is 2.9 dB.

Fig. 2(c) is a plot of the calculated return loss for the helix fed by a 200-Ω transmission line as a function of frequency for the geometry defining frequency of 1.8 GHz. The simulations indicate approximately 70% bandwidth for this structure. For the bandwidth calculation, the criterion used for an acceptable match was a return loss equal to or greater than 10 dB.

B. Square Helices on Handset

In order to analyze a version of the circular helix with a Cartesian grid FDTD code, several square versions were simulated. Fig. 3(b)–(d) represents the schematics of various square approximations to the circular helix seen in Fig. 3(a). All the helical structures shown in Fig. 3 have a pitch height of 0.24λ, a circumference of 0.96λ, and wire radius of $0.001\,395\lambda$. Of the square helices shown in Fig. 3, the structure shown in (d) has the performance most similar to the circular helix.

Fig. 4 illustrates the modification to the standard helix structure shown in Fig. 3(d) mounted on a $0.48\lambda \times 0.48\lambda \times 0.8\lambda$ conducting box. In this square helix structure, all the vertically orientated wire segments are 0.06λ in length and all the horizontally orientated wire segments are 0.24λ in length. This square helix structure has the advantages of easier construction, a geometry easier to integrate with the handset, and can be simulated with a Cartesian grid FDTD code.

Fig. 5(a) and (b) plots the MoM-computed far-field pattern and axial ratio, respectively, for the square helix structure mounted on the small conducting box, as shown in Fig. 4. Fig. 5(c) plots the MoM-computed return loss of this structure when fed by a 200 Ω transmission line as a function of frequency if the geometry-defining frequency is set to 1.8 GHz. The results in Fig. 5(a)–(c) can be compared with plots in Fig. 2(a)–(c) to evaluate the similarity in circuit and radiation performances of the square and circular helices. It can be seen that both of these structures have fairly similar characteristics, although the square helix structure has more directivity and the well-matched impedance region is slightly downshifted in

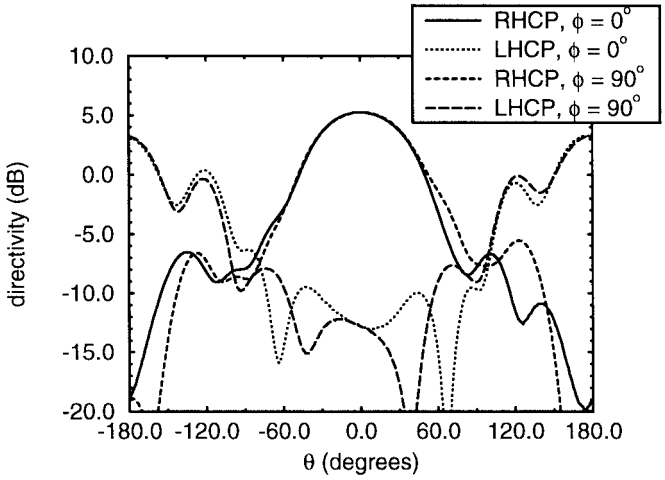

(a)

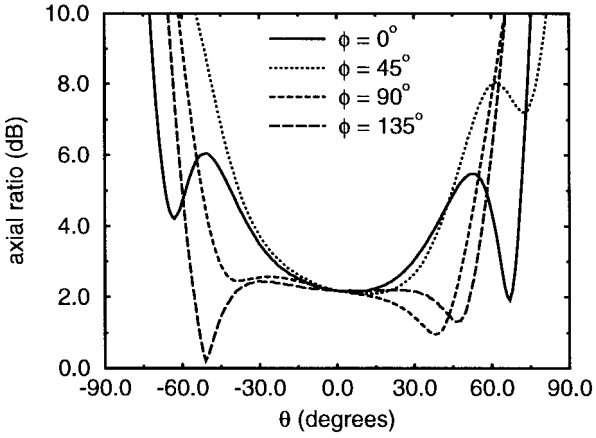

(b)

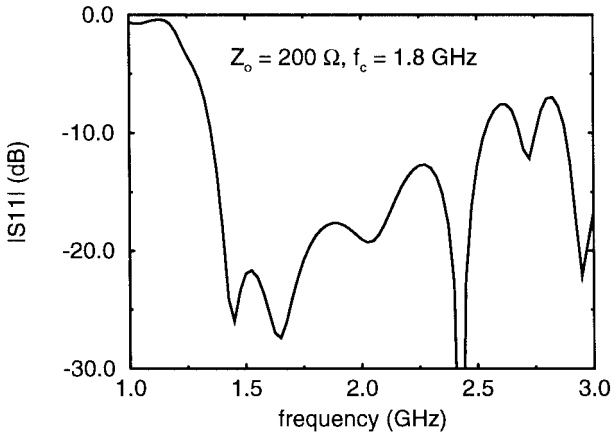

(c)

Fig. 2. MoM-computed electrical performance of the circular helix on a handset illustrated in Fig. 1. (a) Far-field pattern. (b) Axial ratio in decibels, 20 log (major axis/minor axis). (c) Return loss when fed by a 200-Ω transmission for a geometry defining frequency of 1.8 GHz.

frequency. The average axial ratio within the $\theta = 50°$ verticle cone is 2.9 dB for both antennas.

The square helix structure shown in Fig. 4 was also analyzed with FDTD. Fig. 6(a)–(c) provides a direct comparison of the FDTD and MoM-calculated far-field pattern, axial ratio, and return loss for the square helix mounted on the small

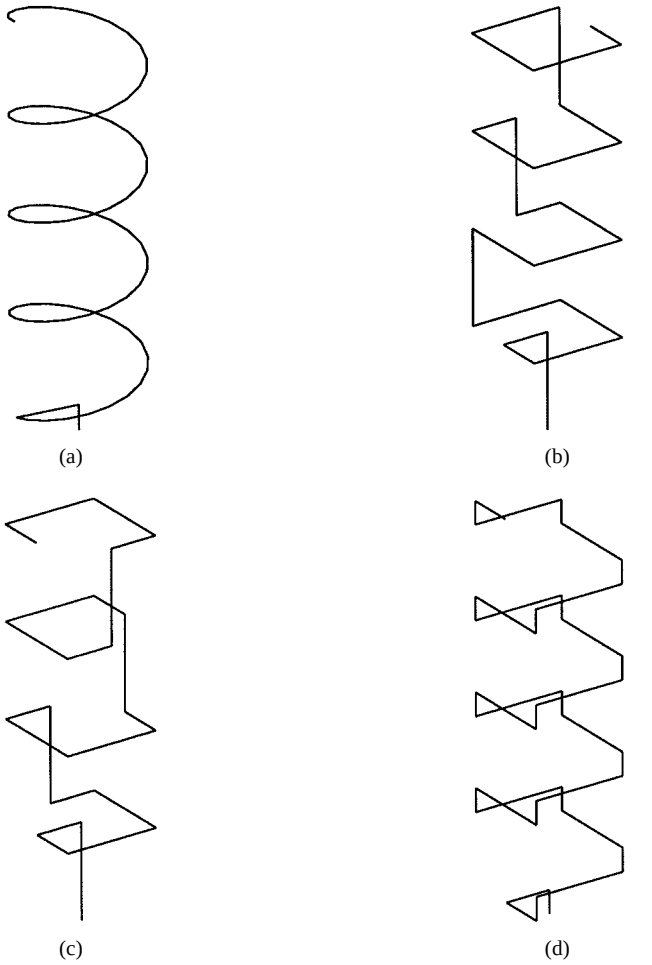

Fig. 3. Four turn helices modeled. (a) Standard circular. (b), (c), and (d) Various square versions. Case (d) has been demonstrated to have performance similar to case (a).

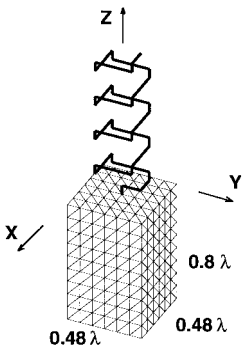

Fig. 4. Schematic of the square helix (perimeter $= 0.96\lambda$, pitch angle $= 14°$, wire radius $= 0.001395\lambda$) mounted on a $0.48\lambda \times 0.48\lambda \times 0.8\lambda$ conducting box.

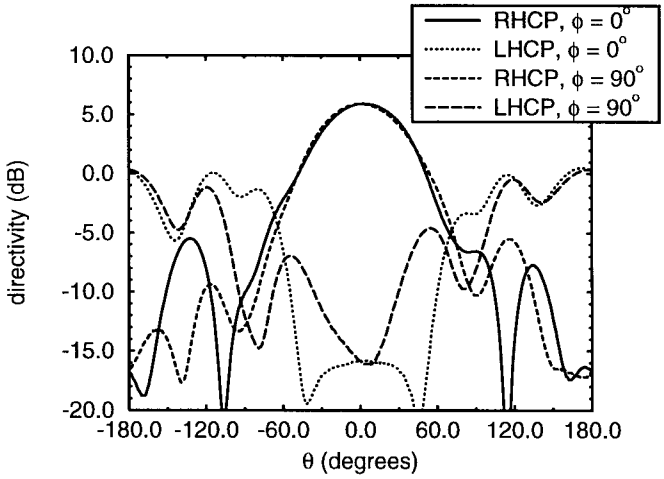

(a)

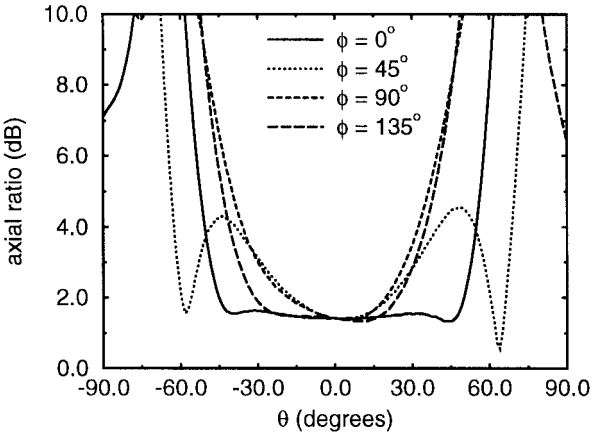

(b)

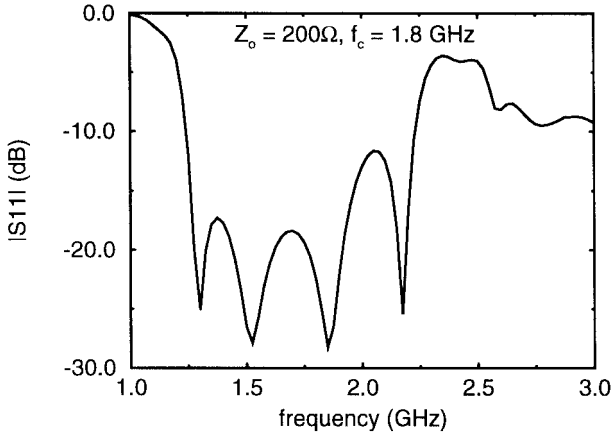

(c)

Fig. 5. MoM-computed electrical performance of the square helix on a handset illustrated in Fig. 4. (a) Far-field pattern. (b) Axial ratio. (c) Return loss when fed by a 200-Ω transmission with a geometry defining frequency of 1.8 GHz.

conducting box. It can be seen from these plots that the FDTD and MoM computations of the square helix on the small conducting box compare very well, especially the pattern. In the MoM simulations, 0.08λ subsectioning of the box and 0.04λ subsectioning of the wire were used. In the FDTD computations, a uniform grid size of 0.02λ was applied.

IV. Biological Tissue Modeling

In [17], a computational head model was included in the FDTD simulations in order to ascertain the impact the user's presence has on the radiation characteristics of the terrestrial personal communication system transceiver at 915 MHz. To construct that head model, a grid with a 6.56-mm spatial resolution was placed on cross-sectional images of the head obtained from an anatomy atlas [23]. Each cell in the grid was then assigned a permittivity and conductivity classification

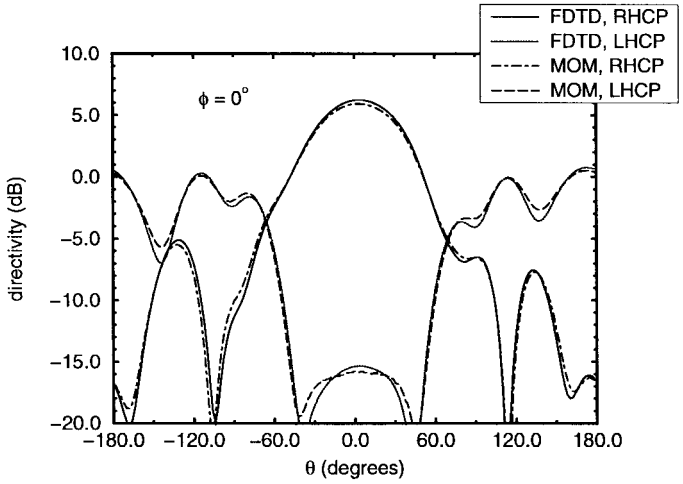

(a)

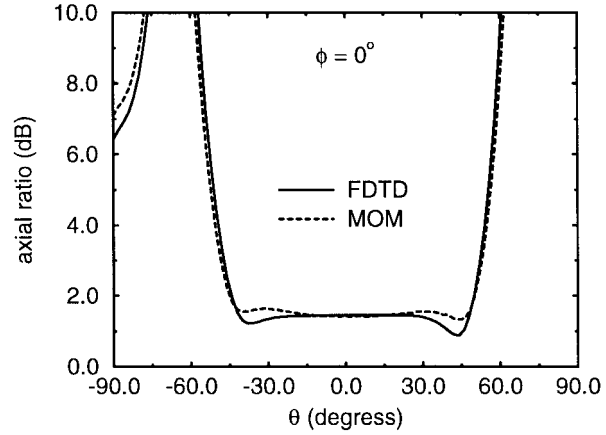

(b)

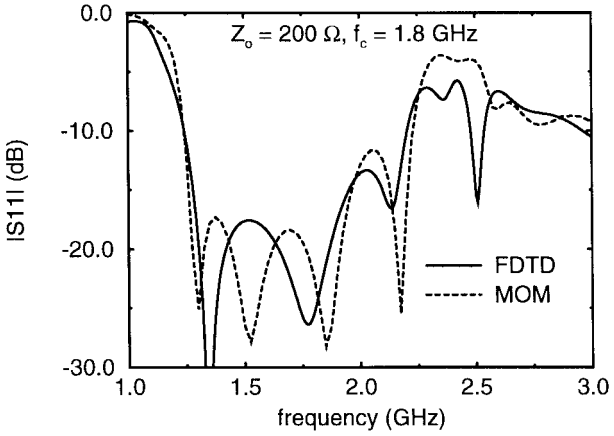

(c)

Fig. 6. Overlays of FDTD and MoM-computed results for the square helix structure on the handset illustrated in Fig. 4. (a) Far-field pattern. (b) Axial ratio. (c) Return loss when fed by a 200-Ω transmission line for a geometry defining frequency of 1.8 GHz.

corresponding to the type of tissue, which filled the majority of the cell. Fig. 7 illustrate a mid-sagittal cross section of the head model.

In this work, a similar computational head model was used to help in the characterization of the personal satellite communication transceiver in close proximity to a user. Although

TABLE I
MATERIAL ELECTRICAL CHARACTERISTICS OF THE COMPUTATIONAL HEAD MODEL AT 1.8 GHz [24]

tissue	Permittivity	Conductivity (S/m)
Bone	8.0	0.15
Skin	32.0	0.57
Muscle	56.0	1.76
Brain	53.0	1.58
Humour	74.0	2.27
Lens	42.0	1.19
Cornea	51.0	2.29

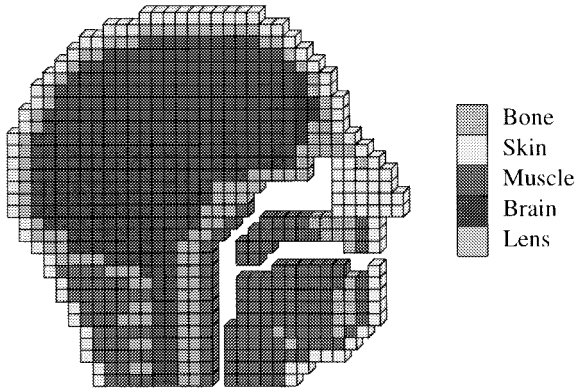

Fig. 7. Mid-sagittal view of the computational head model.

the same structure and approximate head size were used, the electrical parameters of the head model were changed to those of head tissue at 1.8 GHz [24], as shown in Table I. The FDTD grid size used in the included computations was 3.33 mm, which resulted in a head model of approximately 12 000 Yee cells. More detailed head models have been used in FDTD simulations [18]–[21], but it is believed that the finer head detail would cause only small changes to the computed antenna impedance, far-field pattern, and total power-loss calculations [18]–[20].

In this work, the operator's hand was not included. Because the hand does not cover (nor would be positioned close to the antenna element), its effect on the antenna's performance should be minimal [17].

A. Square Helix/Handset Near-Computational Head Model

Fig. 8(a) illustrates the computational head model positioned near the transceiver handset shown in Fig. 4. The frequency of interest is 1.8 GHz, which fixes the FDTD grid size of 0.02λ to 3.33 mm and the size of the transceiver box to 8 cm $\times$ 8 cm $\times$ 13.33 cm. In the computations performed, the handset and head model were spaced two cells apart. Fig. 8(b) and (c) represents schematics in the y-z and x-z cuts of the exact geometry analyzed.

Fig. 9(a) and (b) represents overlays of the far-field pattern and axial ratio results in the $\phi = 0^{\circ}$ cut for the square helix with and without the computational head model present. Fig. 9(c) is an overlay of the computed return loss when fed by a 200-Ω transmission line with and without the head model present. It can be seen in Fig. 9(a) that there are noticeable distortions to the computed far-field pattern due to the presence

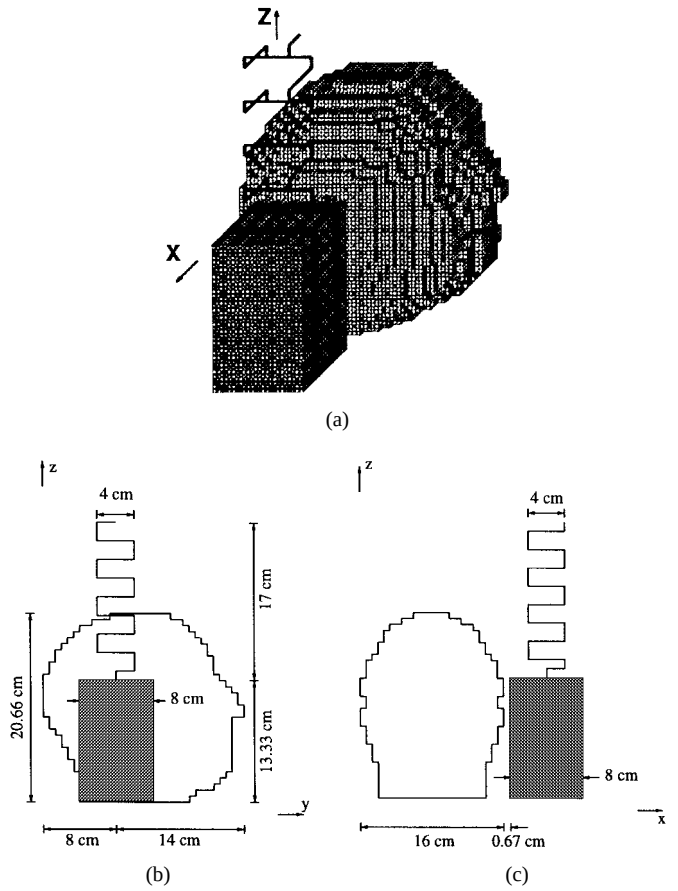

Fig. 8. (a) Illustration of the square helix on a handset positioned near the computational head model. (b) y-z plane cut. (c) x-z plane cut of head model and handset.

of the head model. This, in particular, manifests itself in the poorer axial ratio performance, as seen in Fig. 9(b). In fact, the average axial ratio within the $\theta = 50°$ cone for the square helix antenna on the handset is 2.9 dB as compared to the 9.1 dB when in close proximity to the computational head model. It is also of interest to note that the computed return loss shows only slight changes due to the presences of the computational head. This fact indicates there is only small direct coupling between the antenna and the head model, and that most of the distortion to the far-field pattern is caused by secondary scattering from the head model.

The computations indicate approximately 13% of the total delivered power is dissipated in the head model, which is considerably less than the losses reported in [17]. The decrease in power dissipated in the head model for these simulations when compared to those for the terrestrial personal communication handset is mainly attributed to the greater distance between the head model and the antenna element. In [17], the separation between the handset antenna and head was approximately 2 cm, whereas in the computations presented in this work the separation is approximately 4 cm in addition to the fact the radiating element itself is considerable larger, distributing the radiated power over a larger area.

Fig. 10(a) and (b) shows the computed electric field distribution in the vicinity of the handset—(a) without and (b) with the head model present in the computational domain. Both figures

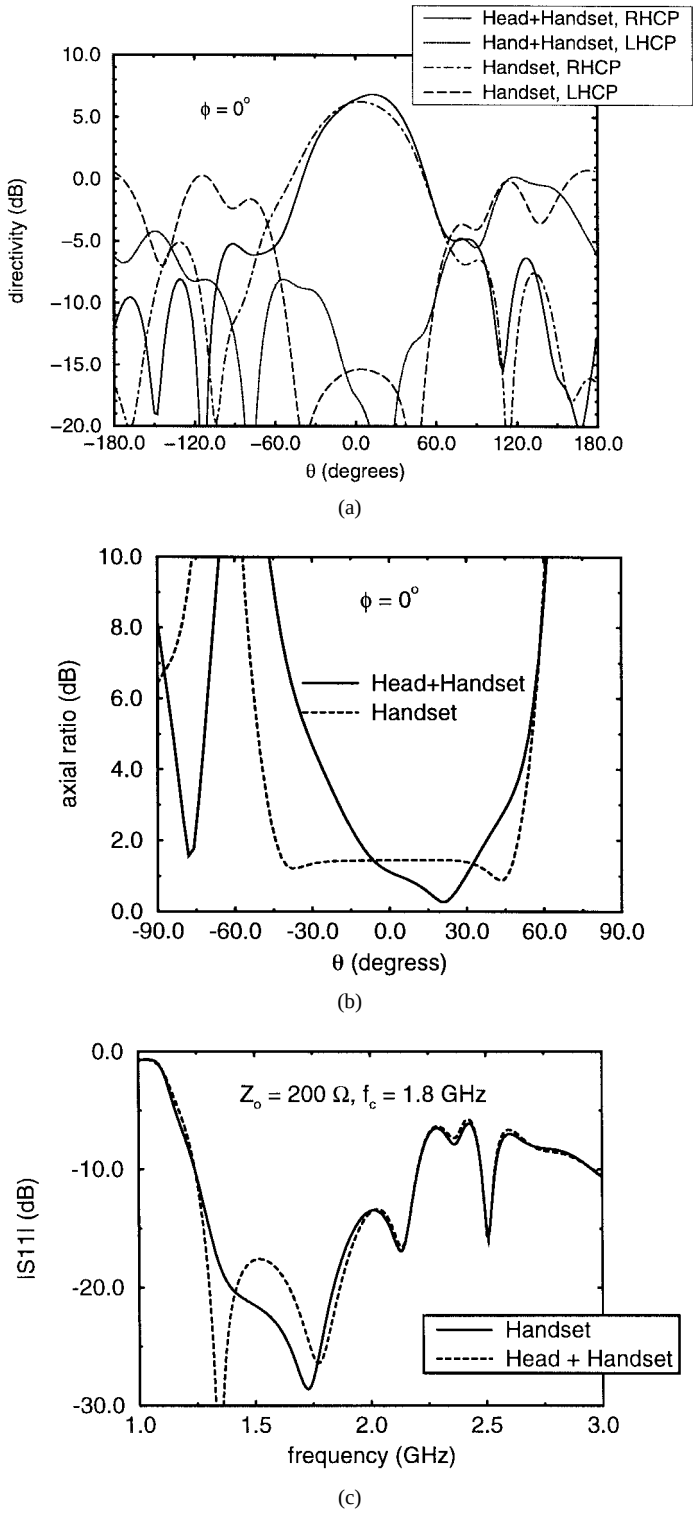

Fig. 9. FDTD computed results for the square helix structure with and without the computational head model present. (a) Far-field pattern at 1.8 GHz. (b) Axial ratio at 1.8 GHz. (c) Return loss when fed by a 200-Ω transmission line. Within the $\theta = 50°$ cone, the average axial ratio raised from 2.9 to 9.1 dB due to the presence of the computation head model.

are plots of the computed electric field in the x-z plane through the exact middle of the handset (see Fig. 4). From Fig. 10(a) and (b), one can see the perturbations of the fields caused by the head's presence. In both figures, the strong electric fields around the radiating wire element are clearly illustrated by

the alternating stair-step circular regions of high-field values. The wire segments further from the feed point, in general, have lower fields surrounding them (as expected) and the field levels are seen to decrease as a function of distance from the wire segments. In Fig. 10(b), the shadowing of the head is visible by the considerably lower field values in the lower left region of the plot when compared to the plot in Fig. 10(a). In addition, the field values in the computational head model are seen to be strongest in the region closest to the radiating element and decrease as they penetrate the head. It is interesting to note the minimal distortion of the field distribution around the wire element caused by the computational head model. This fact illustrates why only small changes are seen in the computed match of the antenna between simulations with and without the head model. This also reconfirms the conclusion that the considerable changes to the far-field radiated pattern caused by the presence of the computation head are more a result of secondary scattering from the head as opposed to direct coupling between the head and radiating element.

SAR is a measure of the power absorbed per unit mass of tissue. This quantity is defined as

$$\text{SAR} = \frac{\sigma}{2\rho}|\mathbf{E}|^2 \tag{1}$$

where ρ is the material density and σ is the material conductivity. Fig. 11 is a contour plot of the computed SAR (for 1-W delivered power) averaged over 1 gm of tissue in the computational head model for this case [17]. Note the predicted SAR distribution in the head decreases with distance from the radiating element, a direct result of the field strength decaying with penetration depth.

One obvious way to reduce the interaction between any handset antenna and the operator is to deploy the elements further away from the operator. As the interaction between the antenna and the operator is reduced, less polarization degradation will be experienced. Because of the extended size of the helix antenna, it inherently exhibits less interaction effects. For smaller circular polarized handset antennas, the operator's presence would be expected to have more significant performance impact. To minimize these impacts, it would be advisable to deploy the element as far away from the operator as possible.

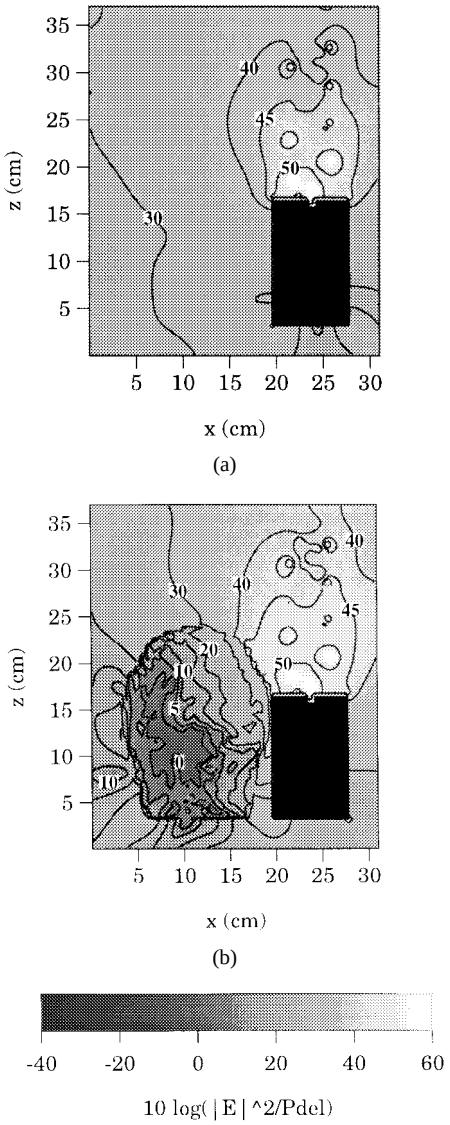

Fig. 10. FDTD computed fields in the vicinity of the handset. (a) Without the head model in the computational domain. (b) With the head model in the computational domain. From these normalized plots, the peak electric field value can be determined. For example, for 1-W delivered power the 5-dB contour is the locus of points where the peak electric field is 1.8 V/m.

V. Conclusion

In this paper, the standard circular helix antenna and a newly introduced square version of the circular helix were studied for application to the personal mobile satellite communication handset. This work employed the MoM and FDTD numerical techniques and the simulations included the effects of mounting the helix on a small conducting box and the close proximity of a human head. The focus was to study the handset antenna circular polarization degradation caused by the close proximity of the operator's head, which would have significant impacts on any satellite communication system design. The helix was selected as a representative circular polarized antenna.

One significant result shown is the similarity in computed performance between a traditional circular helix and a square version thereof. This result facilitated applying the Cartesian grid FDTD technique to the simulation of the helix on the handset. For the square helix, results generated with both the MoM and FDTD techniques are directly compared and a good correlation is observed. This fact yields confidence in the modeling capabilities of each due to the diverse origin of the MoM and FDTD techniques.

Finally, using FDTD the square helix was simulated near a model of a human head. The results indicate the presence of the head model has considerable impact on the circular polarization-radiation purity of the helix, increasing the average axial ratio within the 50° vertical cone from 2.9 to 9.1 dB. This increase in axial ratio is significant enough to affect the overall system link budget. Most of this increase can be attributed to secondary scattering from the head as opposed to direct coupling between the head and the radiating element. This conclusion is supported by the fact the presence of the head model has minimal impact on the computed impedance

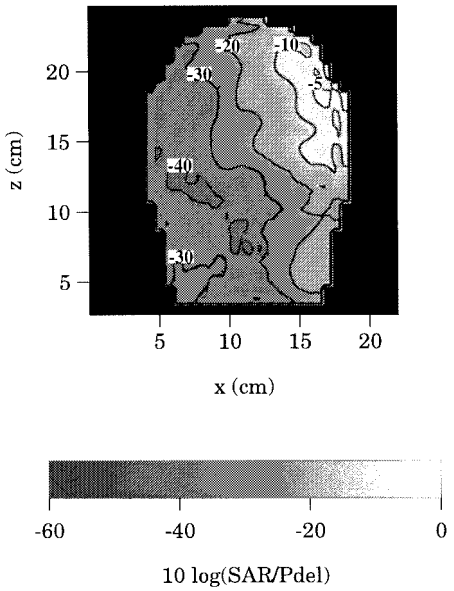

Fig. 11. Computed normalized SAR for the case of the square helix on the handset next to the head model. For 1-W delivered power, the −10-dB contour is the locus of points where the SAR is 0.1 mW/g.

behavior. The results shown are applicable to other circular polarized antennas for the mobile satellite, although for smaller radiators, closer to the head, the coupling between the circular polarized antenna and the human head will be stronger and the polarization degradation even more severe. Clearly, one simple method to maintain high circular polarization purity is to deploy the antenna as far away from the head as possible. Other methods to reduce the polarization degradation caused by the operator's head are currently under study.

ACKNOWLEDGMENT

The authors would like to thank Prof. M. A. Jensen, Brigham Young University, Provo, UT, for many helpful discussions.

REFERENCES

[1] W. W. Wu, E. F. Miller, W. L. Pritchard, and R. L. Pickholtz, "Mobile satellite communications," *Proc. IEEE*, vol. 82, pp. 1431–1448, Sept. 1994.
[2] J. V. Evans, "Satellite systems for personal communications," *Antennas Propagat. Mag.*, vol. 39, no. 3, pp. 7–20, June 1997.
[3] M. A. Jensen and Y. Rahmat-Samii, "Performance of circularly polarized patch antennas for the personal satellite communications including biological effects," in *IEEE Antennas Propagat. Soc. Int. Symp.*, Newport Beach, CA, June 1995, vol. 2, pp. 1112–1115.
[4] J. S. Colburn and Y. Rahmat-Samii, "Quadrifilar-curl antenna for the "big-leo" mobile satellite service system" in *IEEE Antennas Propagat. Soc. Int. Symp.*, Baltimore, MD, July 1996, vol. 2, pp. 1088–1091.
[5] R. F. Harrington, *Field Computation by Moment Methods*. New York: MacMillian, 1968.
[6] E. K. Miller and G. J. Burke, "Low-frequency computational electormagnetics for antenna analysis," *Proc. IEEE*, vol. 80, pp. 24–43, Jan. 1992.
[7] S. M. Rao, D. R. Wilton, and A. W. Glisson, "Electromagnetic scattering by surfaces of arbitrary shape," *IEEE Trans. Antennas Propagat.*, vol. 30, pp. 409–418, May 1982.
[8] H. C. Pocklington, "Electrical oscillations in wires," *Cambridge Phil. Soc. Proc.*, vol. 9, pp. 324–332, 1897.
[9] E. Hallen, "Theoretical investigation into transmitting and receiving qualities of antennae," *Nova Acta Regiae Soc. Sci. Ups. Ser. 4*, vol. 11, pp. 1–44, 1938.
[10] R. E. Hodges and Y. Rahmat-Samii, "An iterative current-based hybrid method for complex structures," *IEEE Trans. Antennas Propagat.*, vol. 45, pp. 265–276, Feb. 1997.
[11] D. E. Livesay and K. Chen, "Electromagnetic fields induced inside arbitrarily shaped biological bodies," *IEEE Trans. Microwave Theory Tech.*, vol. 22, pp. 1273–1280, Dec. 1974.
[12] K. Karimullah, K. Chen, and D. P. Nyquist, "Electromagnetic coupling between a thin-wire antenna and a neighboring biological body: Theory and experiment," *IEEE Trans. Microwave Theory Tech.*, vol. 28, pp. 1218–1229, Nov. 1980.
[13] J. S. Colburn and Y. Rahmat-Samii, "Electromagnetic scattering and radiation involving dielectric objects," *J. Electromagn. Waves Applicat.*, vol. 9, pp. 1249–1277, Oct. 1995.
[14] K. S. Yee, "Numerical solution of the initial boundary value problems involving maxwell's equations in isotropic media," *IEEE Trans. Antennas Propagat.*, vol. 14, pp. 302–307, May 1966.
[15] K. L. Shlager and J. B. Schneider, "A selective survey of the finite-difference time-domain literature," *Antennas Propagat. Mag.*, vol. 37, pp. 39–57, Aug. 1995.
[16] A. Taflove, *Computational Electromagnetics, the Finite-Difference Time-Domain Method*. Boston, MA: Artech House, 1995.
[17] M. A. Jensen and Y. Rahmat-Samii, "EM interaction of handset antennas and a human in personal communications," *Proc. IEEE*, vol. 83, pp. 7–17, Jan. 1995.
[18] M. Okoniewski and M. A. Stuchly, "A study of the handset antenna and human body interation," *IEEE Trans. Microwave Theory Tech.*, vol. 44, pp. 1855–1864, Oct. 1996.
[19] V. Hombach, K. Meier, M. Burkhardt, E. Kühn, and N. Kuster, "The dependence of em energy absorption upon human head modeling at 900 MHz," *IEEE Trans. Microwave Theory Tech.*, vol. 44, pp. 1865–1873, Oct. 1996.
[20] S. Watanabe, M. Taki, T. Nojima, and O. Fujiwara, "Characteristics of the SAR distributions in a head exposed to electromagnetic fields radiated by a hand-held portable radio," *IEEE Trans. Microwave Theory Tech.*, vol. 44, pp. 1874–1883, Oct. 1996.
[21] O. P. Gandhi, G. Lazzi, and C. M. Furse, "Electromagnetic absorption in the human head and neck for mobile telephones at 835 and 1900 MHz," *IEEE Trans. Microwave Theory Tech.*, vol. 44, pp. 1884–1897, Oct. 1996.
[22] C. A. Balanis, *Antenna Theory, Analysis and Design*. New York: Wiley, 1982.
[23] A. C. Eycleshymer and D. M. Schoemaker, *A Cross-Section Anatomy*. New York: D. Appleton-Century, 1911.
[24] P. J. Dimbylow and O. P. Gandhi, "Finite-difference time-domain calculations of SAR in a realistic heterogeneous model of the head for plane-wave exposure from 600 MHz to 3 GHz," *Phys. Med. Biol.*, vol. 36, pp. 1075–1089, Aug. 1991.

Joseph S. Colburn (S'97) received the B.S.E.E. degree (*summa cum laude*) from the University of Washington, Seattle, in 1992, and the M.S.E.E. degree from the University of California, Los Angeles (UCLA), in 1994. He is currently working toward the Ph.D. degree at UCLA.

He is currently employed by TRW Space and Electronics Group, Redondo Beach, CA. Other relevant experience includes interships at the Department of Energy NORCUS program, Richland, WA, U.S. West NewVector, Bellevue, WA, University of Washington Electromagnetics and Remote Sensing Laboratory, Seattle, WA, and Sandia National Laboratories, Albuquerque, NM. His research interests include radiation and propagation issues in wireless communications and related topics in numerical electromagnetics.

Yahya Rahmat-Samii (S'73–M'75–SM'79–F'85), for photograph and biography, see this issue, p. 748.